Article:
Coldstream, J.G., Hutchinson, C.J., Dowding, P.J. et al. (4 more authors) (2025) How Functional Groups Influence Asphaltene Aggregation: Molecular Simulations and Small-Angle Neutron Scattering. Energy & Fuels, 39 (28). ISSN: 0887-0624

https://doi.org/10.1021/acs.energyfuels.5c02091

How Functional Groups Influence Asphaltene Aggregation: Molecular Simulations and Small-Angle Neutron Scattering

Jonathan G. Coldstream,[†] Callum J. Hutchinson,[‡] Peter J. Dowding,[¶] Thomas P. Robinson,[¶] Stephen P. Marsden,[§] David Harbottle,[‡] and Philip J. Camp[*,†]

[†]*School of Chemistry, University of Edinburgh, David Brewster Road, Edinburgh EH9 3FJ, Scotland*

[‡]*School of Chemical and Process Engineering, University of Leeds, Leeds LS2 9JT, UK*

[¶]*Infineum UK Ltd., P.O. Box 1, Milton Hill, Abingdon OX13 6BB, UK*

[§]*School of Chemistry, University of Leeds, Leeds LS2 9JT, UK*

E-mail: philip.camp@ed.ac.uk.

June 19, 2025

Abstract

Asphaltenes are polycyclic aromatic molecules found in high-molecular-weight fractions of crude oil. They dissolve in aromatic solvents like toluene, but not in aliphatic solvents like heptane. Low solubility leads to aggregate formation, and many problems in transport applications. Natural asphaltene fractions contain complex mixtures of molecules which vary widely between sources of crude oil, and so the chemical and structural properties are difficult to characterize. Herein, three synthetic asphaltenes containing different oxidation states of sulfur in binary mixtures of toluene and heptane are studied. Aggregate formation is investigated using a combination of small-angle neutron scattering (SANS) and molecular-dynamics (MD) simulations. The extent of aggregation is found to depend strongly on both the composition of the solvent and the functionality of the sulfur atom. A benzothiophene-functionalized asphaltene, without any oxygen, forms nanoaggregates in toluene that do not change significantly on addition of heptane. In contrast, asphaltenes containing the sulfoxide or sulfone analogs form nanoaggregates in toluene, and much larger clusters above 40% by volume heptane content, with the initial nanoaggregates of the sulfone being slightly larger. Such behavior is apparent in both measured and simulated scattering profiles, and while these techniques probe different length scales, the results are consistent. The microscopic structures of the simulated aggregates are detailed. In systems with low heptane content, the asphaltenes form small clusters of 2–4 molecules, depending on the functionality. In systems with greater heptane content, the sulfoxide and sulfone form larger clusters. The variations in clustering behavior between functional groups and solvents are attributed mainly to the electrostatic interactions between the polar sulfur-containing functional groups, which stabilize 'head-to-tail' configurations in the sulfoxide aggregates, and more complex branched structures in the sulfone aggregates.

1 Introduction

Asphaltenes are polycylic aromatic compounds found in crude oil, and are defined as being soluble in toluene but not in *n*-heptane (hereafter heptane).[1] They find application in bitumen and resins for paving roads and in roofing.[2] They are also the cause of many problems during the process of oil refining, and in applications involving other fractions of crude oil.[3] Asphaltenes form deposits on equipment during oil recovery,[4] and in engines burning less refined fuels, such as large shipping vessels.[5,6] In all cases, asphaltene aggregation and deposition on critical components introduce inefficiencies in equipment, unwanted heat insulation, and in the worst-case scenarios, complete failure due to the build up of deposits.

Despite many advances in the field, the mechanisms of asphaltene aggregation are still a subject of contention.[7] This is partially because asphaltene structures vary widely between samples obtained from different locations around the World, since they are degradation products from a wide range of marine and terrestrial organic matter.[8] In addition, there is likely a combination of molecular effects driving aggregation, which increases the complexity of the problem. Early models of asphaltene aggregation, such as the Yen model[9] and later the Yen-Mullins model,[10,11] attribute cluster formation mainly to π–π stacking. While stacking of aromatic components in the asphaltenes has important geometrical implications for the aggregate structure, these interactions are often too weak to form stable clusters on their own.[12,13] Gray *et al.* stressed the importance of other factors in the assembly of asphaltene aggregates.[14] They argued that ionic interactions between Brønsted acids and bases, hydrogen bonding, and association of apolar, hydrophobic groups play a much greater role in aggregate formation than π–π stacking. It has also been proposed that radical interactions could enhance the thermal stability of aggregates.[15]

The most prominent feature of asphaltenes is their large aromatic component, but they also contain aliphatic chains, and heteroatoms such as nitrogen (0.6–3.3%), oxygen (0.3–4.9%), and sulfur (0.3–10.3%) in various forms.[16] Sulfur is an important element in asphaltenes, as it appears in many different chemical environments and oxidation states,[17,18]

and can make up as much as 10 wt% of some asphaltenes,[19–21] although the average content is around 4–6 wt%. Here, the focus is on the effect of different sulfur-containing heterocyclic groups, and how they affect aggregation. The sulfur groups considered are S, SO, and SO_2, all in five-membered rings. Using X-ray absorption near-edge structure (XANES) spectroscopy, Mitra-Kirtley *et al.* and Pomerantz *et al.* found that the thiophene group (S) is by far the most common sulfur-containing heterocyclic motif in some asphaltenes, while the corresponding sulfoxide (SO) and sulfone (SO_2) are far less abundant.[19,20] Broadly similar proportions of these groups are found in different samples,[21] but the details depend on geographical location and drilling well depth. Noting the relative abundances of S and O,[16] and that oxygen can be found in many other functional groups (such as ethers, carbonyls, hydroxides, etc.), thiophenes should be more abundant than the oxidized versions. Nonetheless, the effects of a particular species in a mixture can be out of proportion to its abundance, and in addition, oxidation can occur during air-injection oil recovery,[22] or in use.[23]

To explore the effects of heterocyclic sulfur oxidation, the simple *model* asphaltenes shown in Figure 1 have been synthesized and characterized. The synthetic and chemical characterization work will be reported in a dedicated article.[24] The sulfur atom is present in benzothiophene, benzothiophene sulfoxide, and benzothiophene sulfone functional groups. For brevity, the model asphaltenes will be referred to as 'thiophene', 'sulfoxide', and 'sulfone', respectively, throughout this work. An important structural feature of the sulfoxide and sulfone molecules is that the O atoms are not in the plane of the five-membered heterocycle: in sulfoxide, the O atom is below the plane; and in sulfone, one O atom is below and the other is above the plane.

In this work, the aggregation of the different model asphaltenes in binary mixtures of toluene and heptane are elucidated by a combination of small-angle neutron scattering (SANS) experiments and atomistic molecular-dynamics (MD) simulations, and the effects of the oxidation state of the sulfur atom are determined and explained. This is a particularly powerful combination of techniques. SANS–and small-angle X-ray scattering (SAXS)–

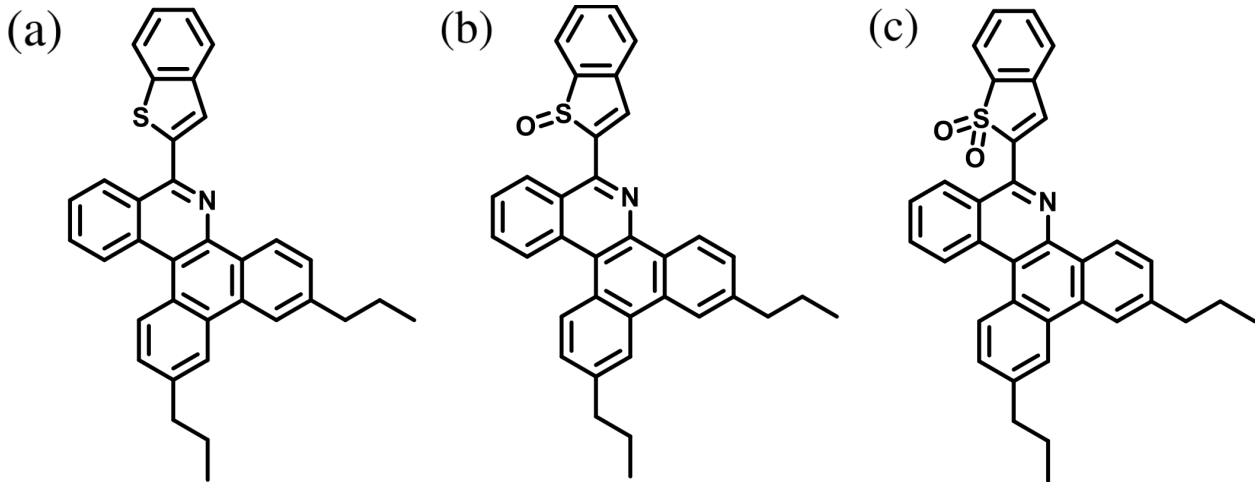

Figure 1: Structures of the studied asphaltenes: (a) 'thiophene'; (b) 'sulfoxide'; (c) 'sulfone'.

provides information on the large-scale structures of clusters.[25,26] The interpretation of scattering measurements relies on some kind of assumed model, but it is possible to infer the existence of interesting structures, such as core-shell aggregates with the core consisting of the planar rings and the shell consisting of aliphatic side chains. Atomistic MD simulations are generally limited to relatively small structures, and a minimum wave vector $q_{\min} \sim 2\pi/L$, where L is the size of the simulation box. Measured and computed scattering profiles can be spliced together, with some overlap, to provide information over a wide range of wave vectors, q. Unfortunately, the degree of overlap in q is bound to be quite small, because of the experimental and computational limitations. Nonetheless, an attempt is made here to compare measured and simulated SANS profiles directly. Once it has been confirmed that the simulated scattering is at least consistent with the measured one, then the atomic-scale structures from the simulations can be visualized and characterized to provide a reliable description of the aggregates.

Previous simulation studies have been performed with one or more types of asphaltenes, with the aim of mimicking the wide range of species found in natural samples. In a series of studies, Santos Silva *et al.* systematically changed the asphaltene architecture and chemical composition,[27–30] and added other species such as porphyrins,[31] to explore the effects of specific molecular features on aggregation. Concerning the effects of heteroatoms, structures

containing N, NH, O, and S (with each heavy atom bonded only to carbon) have been of particular interest, and the polarity of such groups is a key factor in driving aggregation. Typically, anywhere between 2 and 135 asphaltene molecules were used in the simulations along with the united-atom GROMOS96 force field (53a6 parameter set). The effects of solvent have also been explored, being either pure toluene[27–29] or some combination of toluene, heptane, and water.[30,31] Note that, in these studies, any sulfur was restricted to be of the thiophene type, i.e., not oxidized. The all-atom OPLS force field was used by Headen *et al.* to examine the clustering, and potentials of mean force, in systems containing 27 large asphaltene molecules of various types, either in pure toluene or pure heptane.[32] Immense, microsecond-long simulations containing about 10^3 asphaltene molecules and over 10^5 solvent molecules, all described with a united-atom force field, were carried out by Javanbakht *et al.*[33] These calculations confirmed the existence of two types of aggregation–nanoaggregation and clustering–distinguished not only by size but also by fractal dimension. All-atom MD simulations of deasphalting were carried out by Park *et al.*, in which the addition of a light solvent (*n*-pentane) leads to extractant-rich and asphaltene-rich phases. The effects of polydispersity on asphaltene aggregation, and how to simulate them efficiently using machine-learned representative molecules described with the all-atom GAFF force field, were detailed by Pétuya *et al.*[34]

While naturally occurring asphaltenes are relevant in many applications, it is difficult to pinpoint which structural motifs are the most responsible for aggregation because of the complexity and polydispersity of the solutions. Simulations of the type described above provide some vital insights on this problem. Knowledge of the interactions between specific functional groups and how these drive aggregation is essential when designing dispersants, which are molecular additives that slow down or even prevent aggregation. The effectiveness of certain dispersants is known, but the mechanisms by which they act remain relatively poorly studied.[35–38] Simulations provide details on the molecular interactions, which have important implications for the design of new and more effective dispersants.[39] Hence, the

use of atomistic simulations in this work is motivated by the need to understand the specific roles of different functional groups, in this case S, SO, and SO_2.

The overall aims of the current work are to use experiments and simulations to determine the solvent conditions for aggregation of asphaltenes containing sulfur in various oxidation states, and provide detailed structures of the resulting clusters. The asphaltenes are found to form small clusters of 2–4 molecules in systems with high toluene content, and aggregate further into nanoaggregates in systems with high heptane content. In clustered systems, disordered stacks–the nanoaggregates–stick together to form larger clusters, even with the limited number of molecules available in the simulations. Simulated neutron scattering profiles are compared to, and complement, experimental data since they cover different ranges of q. Aggregation is found to have a strong dependence on the oxidation state of the sulfur, with more polar functional groups inducing aggregation at a lower volume fraction of heptane. The specific interactions between functional groups are revealed using simulations by calculating radial distribution functions (RDFs).

The rest of the article is organized as follows. The models and methods are presented in Section 2, which covers both the simulations (2.1) and the brief details of the experiments (2.2).[24] Section 3 contains results and discussion of simulation snapshots (3.1), measured and simulated SANS profiles (3.2), and simulated RDFs (3.3). Section 4 concludes the article.

2 Models and Methods

2.1 All-Atom Simulations

The OPLS-AA force field was used to describe the interactions within the asphaltenes and the solvent.[40,41] This force field has been used with success in other simulation studies, involving different asphaltenes in both toluene and heptane.[32,33,39] In this study parameters were taken from the Tinker (OPLSAA08)[42,43] parameter set. Standard parameters can also be accessed conveniently using other online resources such as LigParGen.[44–47] A link to a

sample LAMMPS input file, and sample LAMMPS data files containing bonded and non-bonded parameters for each asphaltene in 2:8 heptane:toluene mixtures, is given at the end of the article. The non-bonded Lennard-Jones (LJ) interactions were cut off at 12 Å, and the long-range electrostatic interactions were calculated with the particle-particle particle-mesh method. In all cases, the system was simulated in the NVE ensemble for 0.1 ns with a timestep of $\delta t = 0.1$ fs, followed by 0.25 ns in the NVT ensemble with $\delta t = 0.5$ fs, and finally 100 ns in the NPT ensemble with $\delta t = 1$ fs. Structural properties were calculated at intervals of 1 ns from the last 40 ns of the NPT simulation. Where applicable, the temperature and pressure were set to 298 K and 1 atm, respectively, and controlled using the Nosé-Hoover thermostat and barostat. The equations of motion were propagated using the velocity-Verlet algorithm. Initial configurations were generated using PACKMOL.[48] Simulations were performed using LAMMPS,[49,50] with the GPU acceleration package.[51]

The numbers of molecules used in each simulation are given in Table 1. In each case, 30 asphaltene molecules were used, which naturally limits the aggregation number. The numbers of solvent molecules correspond to the given volume ratios, and with 5 wt% asphaltene; for these calculations, the molar volumes of heptane and toluene at 298 K are, respectively, 1.4744×10^{-4} m^3 mol^{-1} and 1.0686×10^{-4} m^3 mol^{-1}.[52] A higher mass percentage of asphaltenes is used in simulation than are found in the experiments, which measure around 0.5−1.0 wt%, but this keeps the total number of atoms in the systems computationally feasible to simulate. This is not an unrealistic weight percentage, with some heavy fuel oil samples reaching almost 15 wt% in asphaltene content.[53] The increase in concentration will affect the conditions under which the molecules aggregate, however the structures of the individual aggregates should still be comparable to those found in the experimental systems; this is justified by comparison to experimental results.

Table 1: The number of each type of solvent molecule included in the simulations. Each simulation also contains 30 asphaltene molecules at 5 wt%.

asphaltene	heptane:toluene by volume	N_{heptane}	N_{toluene}
thiophene	0:10	0	3067
thiophene	2:8	464	2561
thiophene	4:6	972	2010
thiophene	6:4	1528	1404
thiophene	8:2	2141	738
thiophene	10:0	2820	0
sulfoxide	0:10	0	3165
sulfoxide	2:8	479	2644
sulfoxide	4:6	1003	2074
sulfoxide	6:4	1578	1450
sulfoxide	8:2	2210	762
sulfoxide	10:0	2911	0
sulfone	0:10	0	3264
sulfone	2:8	494	2727
sulfone	4:6	1035	2139
sulfone	6:4	1627	1495
sulfone	8:2	2279	786
sulfone	10:0	3002	0

2.1.1 Radial Distribution Functions

Radial distribution functions (RDFs) of atoms within the asphaltene provide important information about the structure of the aggregates. For non-identical particles, the RDF is defined as

$$g_{ab}(r) = \frac{V}{N_a N_b} \left\langle \sum_{i=1}^{N_a} \sum_{j=1}^{N_b} \delta(r_{ij} - r) \right\rangle \tag{1}$$

where V is the volume of the simulation box, r_{ij} is the distance between particles i and j, and N_a and N_b are the total numbers of particles of type a and b, respectively. If the particle types are identical, i.e., if $a = b$, then terms of the sum with $i = j$ are excluded, and the normalisation factor becomes $\frac{V}{N(N-1)}$. The angled brackets $\langle \ldots \rangle$ denote an ensemble average.

2.1.2 Structure Factors

Small-angle neutron scattering (SANS) is a powerful technique for investigating the structures of asphaltenes and their aggregates, and is a natural choice since the accessible neutron wavelengths are of a similar length scale to the asphaltene molecules and aggregates.[54] Structural information can be obtained from the form of the wave vector-dependent scattering intensity, $I(q)$, which is proportional to the structure factor $S(q)$. The structure factor can be computed in simulations by

$$S(\boldsymbol{q}) = \left\langle \left| \sum_{j=1}^{N} b_j e^{-i\boldsymbol{q}\cdot\boldsymbol{r}_j} \right|^2 \right\rangle, \tag{2}$$

where N is the total number of asphaltene atoms, and b_j and $\boldsymbol{r}_j$ are, respectively, the neutron scattering length and the position vector of atom j. $\boldsymbol{q}$ is the scattering wave vector, which must be commensurate with the periodic boundary conditions of the cubic simulation box, and hence $\boldsymbol{q} = (2\pi/L)(n_x, n_y, n_z)$, where L is the box length, and $n_\alpha = 0, \pm1, \pm2, \ldots$ Since the solution is isotropic, the scattering intensity depends only on $q = |\boldsymbol{q}|$, and so the results for wave vectors with the same q are averaged. In this work, the structure factor is calculated from the asphaltene molecules only. The physical assumption behind this is that the solvent mixtures are homogeneous and isotropic, and so the scattering arises solely from density fluctuations associated with the asphaltene molecules and aggregates. This is a good approximation for the low-q portion of $S(q)$, since the corresponding real-space structures are on length scales $\sim 2\pi/q$. Hence, atom-sized structures dominate $S(q)$ in the region of $q > 1$ Å^{-1}, and larger-scale structures dominate $S(q)$ at lower wave vectors.

2.2 Experimental Methods

The molecules shown in Figure 1 were synthesized as part of a wider suite of molecules. The thiophene was obtained by Suzuki coupling of benzothiophene-2-boronic acid with the corresponding dibenzophenathridinyl bromide, available through a four-step sequence from

commercial materials. The sulfoxide and sulfone were prepared by oxidation of the thiophene using *meta*-chloroperoxybenzoic acid. All compounds were characterized using ^{1}H and ^{13}C NMR, and high-resolution mass spectrometry. Full details of the synthesis and characterization of these and related compounds will be disclosed separately.[24]

SANS measurements were performed on beamline D33 at the Institut Laue-Langevin (ILL, Grenoble) as described in ref 24. Model compound solutions were prepared either by dissolving 10 g L^{-1} of sample in 1.5 mL of toluene-d8 (99 atom % D) or 5 g L^{-1} of sample in 3 mL of a 1:1 (v/v) mixture of heptane-d16 and toluene-d8 ('heptol-d'). Each solution was sonicated (200 W ultrasonic bath, VWR) for 5 minutes before being transferred into 1400 μL cylindrical quartz cells (Type 120-QS, Hellma). Scattering was conducted at 25 °C using a fixed detector distance of 10 m, a neutron wavelength $\lambda = 4.6$ Å (FWHM $\simeq 10\%$), and a corresponding q range of roughly 0.0015–0.4 $Å^{-1}$. Collection times were set to 300, 900, or 1800 seconds depending on scattering intensity and signal quality.

3 Results and Discussion

The results are organized as follows. First, MD simulation snapshots will be analyzed visually, showing the hierarchical structures of the aggregates (Section 3.1). Cluster distributions will be presented to provide additional detail. The simulated structure factors will then be compared to experimental SANS data, and interpreted with reference to the simulation snapshots (Section 3.2). Finally, RDFs of the sulfur and oxygen atoms within the asphaltene molecules will be presented, and these characterize the internal structures of the nanoaggregates (Section 3.3). Results for all asphaltenes and all solvent compositions will be presented in each section.

3.1 Simulation Snapshots

Figure 2 shows simulation snapshots of the thiophene asphaltenes in (a) toluene and (b) heptane. The first interesting point is that the two snapshots are quite similar, showing that the solvent does not have a strong effect on aggregation. In both solvents the asphaltenes form small aggregates of two or three asphaltene molecules, with the aromatic planes parallel to one another. These small disordered stacks are known as 'nanoaggregates' in the Yen-Mullins model.[11] There is little secondary aggregation of the nanoaggregates to form larger clusters. The sulfur atoms appear to be close to each other in the nanoaggregates, possibly as a result of the van der Waals forces between large, polarizable atoms (encoded in the LJ interaction parameters). It could also be that, since the molecules are not completely flat, their geometries are more compatible when they are similarly oriented.

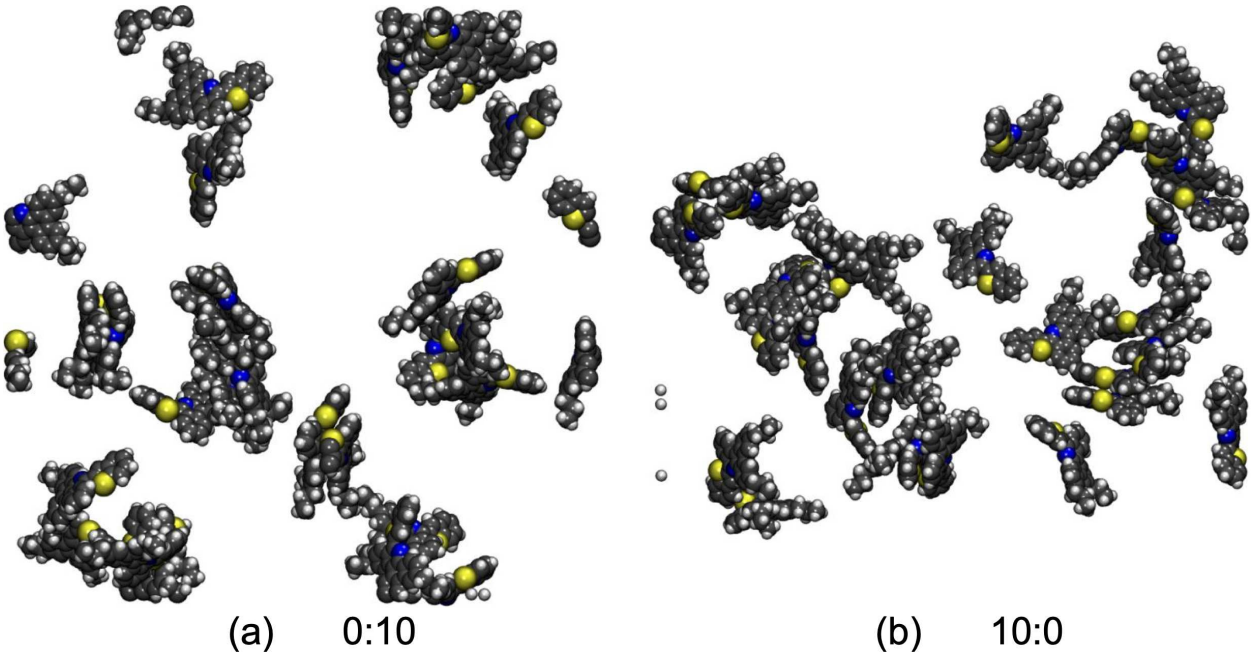

Figure 2: Simulation snapshots of the thiophene asphaltenes in (a) toluene and (b) heptane after 100 ns of simulation. The atoms are shown with a space filling representation with the colors as follows: hydrogen – white; carbon – gray; nitrogen – blue; sulfur – yellow. The solvent is not shown for clarity.

Cluster distributions for the thiophene asphaltenes in toluene and heptane are presented in Figure 3(a) and (b), respectively. Molecules were identified as being part of the same

cluster if any two atoms on different molecules were within 3.5 Å of one another, which is the criterion proposed by Headen *et al.*[32] In both solvents, the cluster probability p_n is a rapidly and monotonically decaying function of cluster size n. Two statistics are given in Figure 3: the number average of the cluster size, or aggregation number, $\langle n \rangle = \sum_n np_n$; and the 'mass average' of the cluster size, given by

$$\langle m \rangle = \frac{\sum_n n^2 p_n}{\sum_n np_n} = \frac{\langle n^2 \rangle}{\langle n \rangle}. \tag{3}$$

$\langle m \rangle$ is equivalent to the average size of a cluster in which a randomly selected molecule is located. Both $\langle n \rangle$ and $\langle m \rangle$ are small in each case, which shows that the degree of aggregation is low.

Figure 4 shows the sulfoxide asphaltene in toluene, heptane, and mixtures. In toluene and the 2:8 heptane:toluene mixture, the sulfoxide asphaltenes form stacks of approximately 2–3 molecules. In the 4:6 heptane:toluene system, larger nanoaggregates of 4–5 asphaltene molecules have formed, and have begun to aggregate further, creating a loose and extended cluster. This is very different behavior to the thiophene system, and introducing a polar functional group has driven aggregation to a greater extent. The 6:4, 8:2, and heptane systems contain one or two large aggregates, which are in equilibrium with a small number of free asphaltene molecules. The polar sulfoxide groups can arrange themselves, head-to-tail, into chains within the stacks of asphaltenes, and one of these is clearly visible in Figure 4(e). The dramatic difference between the thiophene and sulfoxide asphaltenes suggests that the electrostatic interactions between the sulfoxide groups play an important role in aggregation. The specific correlations between S and O atoms are analyzed in detail in Section 3.3.

Cluster distributions for the sulfoxide asphaltenes in toluene and heptane are presented in Figure 3(c) and (d), respectively. In toluene, p_n decays monotonically with increasing n. In heptane, p_n has an additional feature which indicates some larger aggregates in the region of $n = 20$. Restricting the average to aggregates with $n \geq 15$ gives $\langle n \rangle = 20.8$. For

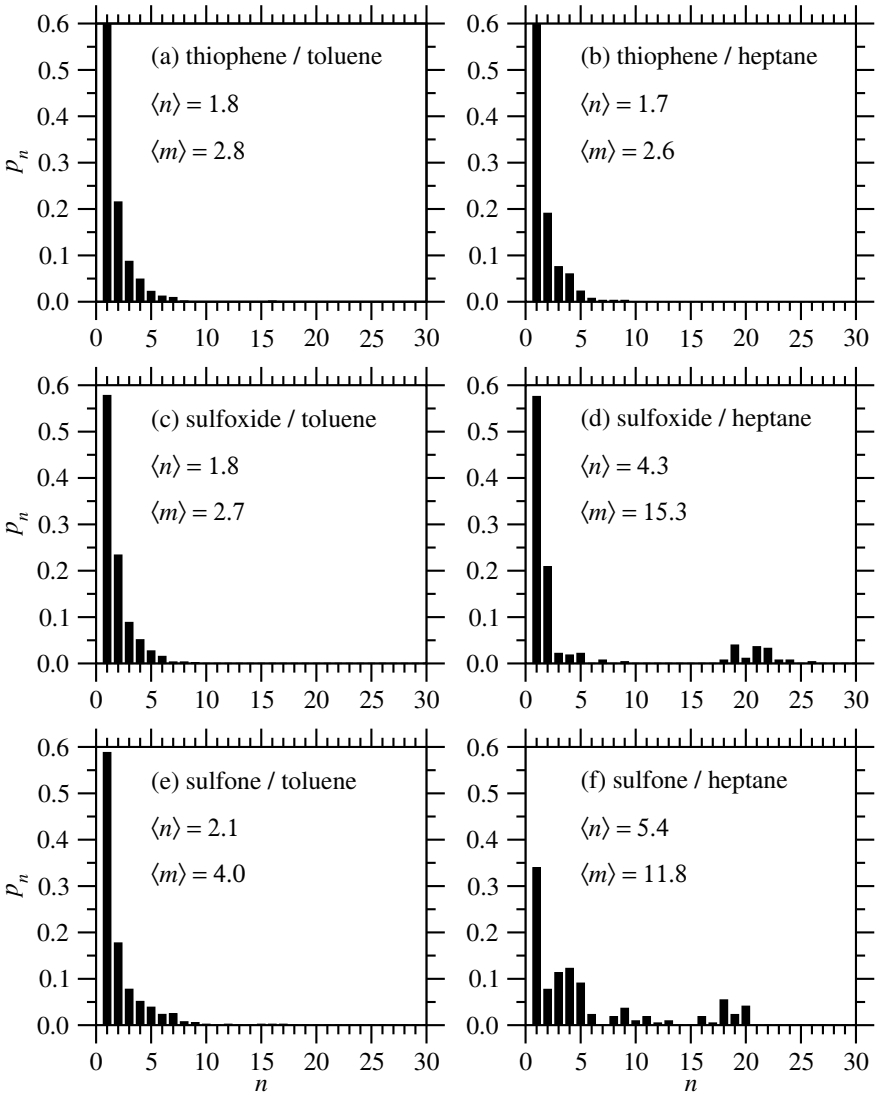

Figure 3: Cluster distributions for different asphaltenes in pure toluene and pure heptane: (a) thiophene in toluene; (b) thiophene in heptane; (c) sulfoxide in toluene; (d) sulfoxide in heptane; (e) sulfone in toluene; (f) sulfone in heptane. Also shown in each panel are the number-averaged cluster size $\langle n \rangle$, and the mass-averaged cluster size $\langle m \rangle$.

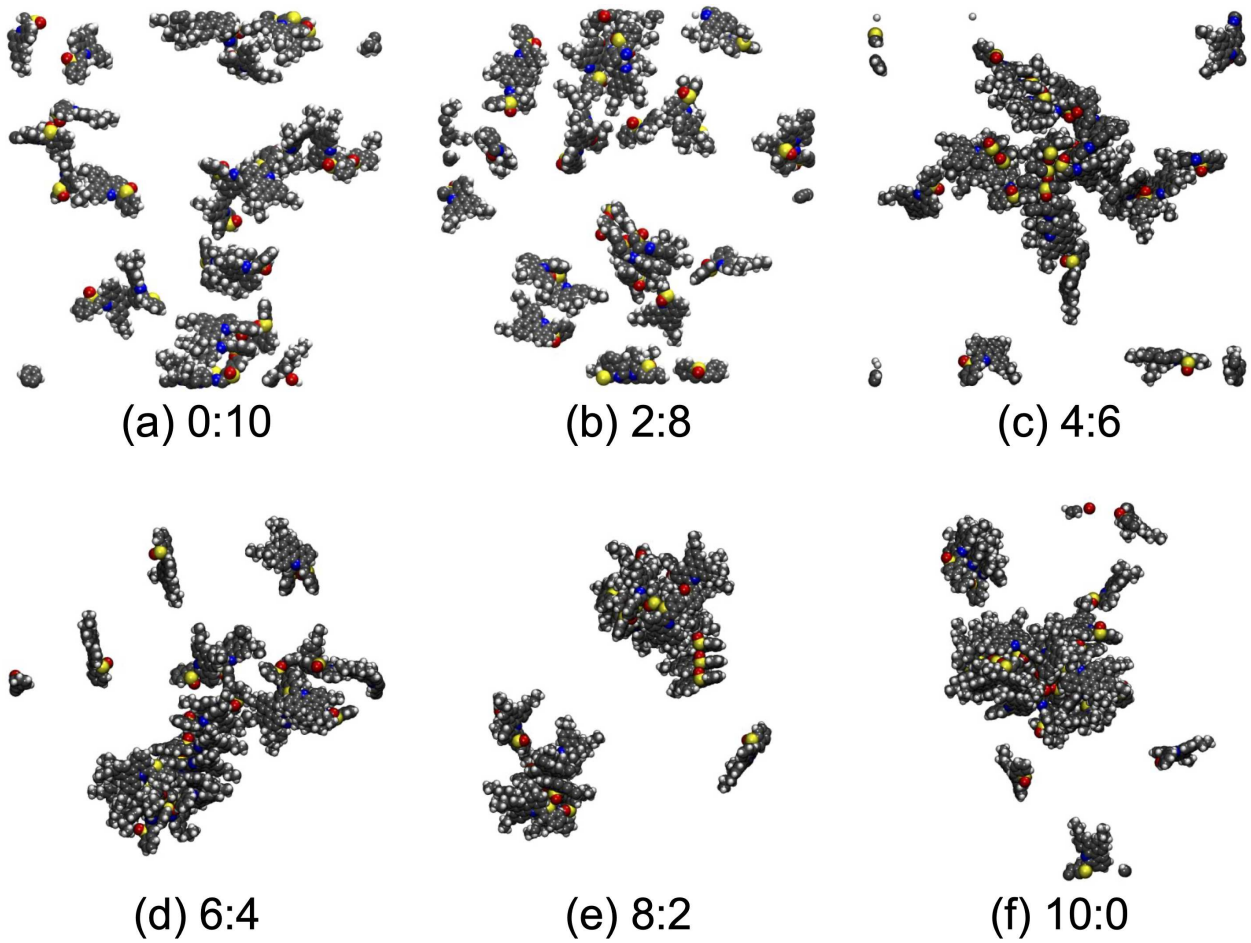

Figure 4: Simulation snapshots of sulfoxide asphaltenes in mixtures of heptane and toluene after 100 ns of simulation. The heptane:toluene volume ratio is shown in the sub-caption of each image. The atoms are shown using a space filling representation with the colors as follows: hydrogen – white; carbon – gray; nitrogen – blue; oxygen – red; sulfur – yellow.

the overall statistics, both $\langle n \rangle$ and $\langle m \rangle$ signal the formation of well-defined, large aggregates when the solvent is switched from toluene to heptane.

Short-range interactions between polar atoms are clearly important in stabilizing the clusters. Naïvely, taking the solvent to be a dielectric continuum, the relative strengths of the electrostatic interactions could be obtained from Coulomb's law. Toluene has a relative dielectric permittivity of $\epsilon = 2.38$, while for heptane $\epsilon = 1.96$.[55] With all other variables being equal, the ionic interactions would be proportional to ϵ^{-1}, and hence around 20% stronger in heptane than in toluene, making cluster formation in heptane easier than in toluene. Since the polar atoms are in close contact, a more realistic explanation is that the slightly more polar toluene solvates the polar functional groups better than does heptane, which means that aggregation is disfavored in toluene. It is difficult to attribute much of the changes in clustering between solvent compositions to toluene disrupting the π–π stacking, because the thiophene system shows very little variation between the two pure solvents.

Figure 5 shows simulation snapshots of sulfone asphaltenes in varying volume ratios of heptane and toluene. In Figure 5(a), some small aggregates have formed in pure toluene, which appear slightly larger than in the sulfoxide system. In Figure 5(b), 2:8 heptane:toluene, the situation is similar to in pure toluene with small nanoaggregates. In 4:6 heptane:toluene [Figure 5(c)], larger clusters of the nanoaggregates have begun to form, but there are still many free molecules. Almost complete aggregation has occurred in 6:4 heptane:toluene [Figure 5(d)] with one very large stack of 10 molecules visible alongside a cluster of several smaller nanoaggregates. The behavior is similar in Figures 5(e) and (f), with larger clusters made up of smaller nanoaggregates, and the majority of nanoaggregates containing approximately 4–5 molecules. As with the sulfoxide asphaltene, electrostatic interactions seem to play a key role in the formation of larger clusters.

Cluster distributions for the sulfone asphaltenes in toluene and heptane are presented in Figure 3(e) and (f), respectively. In toluene, p_n decays monotonically with increasing n, just the same as with the other two asphaltenes. In heptane, p_n shows a broad distribution of

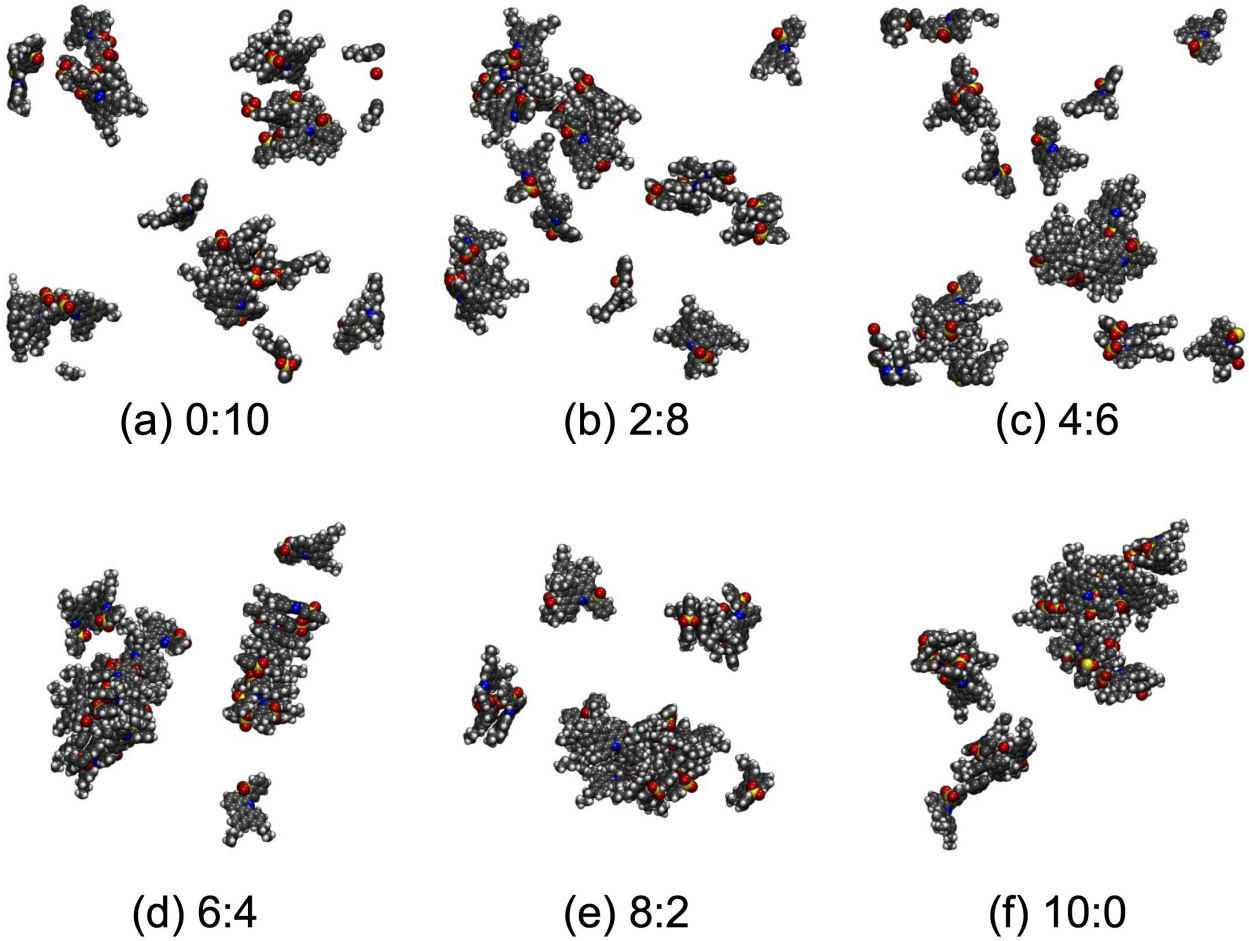

Figure 5: Simulation snapshots of sulfone asphaltenes in mixtures of heptane and toluene after 100 ns of simulation. The heptane:toluene volume ratio is shown in the sub-caption of each image. The atoms are shown using a space filling representation with the colors as follows: hydrogen – white; carbon – gray; nitrogen – blue; oxygen – red; sulfur – yellow.

aggregate sizes up to $n = 20$, with a less distinct large-aggregate portion as compared to the sulfoxide asphaltenes. Restricting the average to aggregates with $n \geq 15$ gives $\langle n \rangle = 18.5$. The overall changes in $\langle n \rangle$ and $\langle m \rangle$ are not quite as pronounced as they are with the sulfoxide asphaltenes, due to the presence of intermediate-sized aggregates.

In all cases the clusters and nanoaggregates are dynamic and are constantly exchanging molecules with free asphaltene molecules in solution, or other clusters. As there are only 30 asphaltene molecules in each case, the extent of the clustering could be limited by the number of molecules in solution. In any case, the apparent degree of aggregation easily reaches a steady state on the time scale accessed here.

3.2 Small-Angle Neutron Scattering

In this section, simulated structure factors calculated using eq 2 are compared to experimental measurements by SANS. Results for all three asphaltenes are considered. One small issue is that some simulations were carried out at 4:6 and 6:4 heptane:toluene volume ratios, while some experiments were performed with a 5:5 volume ratio, but the differences are small. In any event, simulation results for 4:6 and 6:4 compositions happen to be very similar, and can be assumed to bracket results for the 5:5 composition. The comparison of the simulated $S(q)$ with the experimental $I(q) \propto S(q)$ is achieved by scaling, but not shifting, the experimental results, since the asphaltene concentrations are different in each case, and the experimental results are for the total scattering. SANS experiments and MD simulations probe quite different length scales, and the degree of overlap in the measured and calculated $S(q)$ is quite small. On the one hand, this is beneficial, as the techniques provide complementary information. On the other hand, the lack of overlap means that it is difficult to validate molecular-level spatial correlations predicted in the simulation model and/or provide much insight on the scattering at very low wave vectors (corresponding to large structures). As a result, the comparison between experiment and simulation is limited to consistency in the small overlapping region of q which, after scaling, means similarities in

the gradient and curvature of $S(q)$.

Figure 6 shows the scattering intensity as a function of wave vector for the thiophene asphaltene [Figure 1(a)] in toluene, heptane, and intermediate mixtures. The experimental data are compared to the closest simulated solvent composition. The simulated solvent compositions are not exactly the same as the experiment, however above a threshold aggregation concentration of heptane, the scattering profiles are all very similar. This implies that changing the solvent above this point makes very little difference to the aggregate structure. Peaks in $S(q)$ correspond to structures in real space with an approximate size $2\pi/q$, giving direct structural information about the system. In all solvents, the thiophene systems are visually similar, and therefore the scattering profiles are also similar. In toluene, the experimental and simulated profiles match up well in the overlapping q range. The drop in $S(q)$ at $q \simeq 0.3$ Å^{-1} corresponds to a real-space density fluctuation of about 20 Å, approximately the width of an asphaltene molecule. The π–π stacking distance, about 4 Å, gives rise to the broad feature at $q \simeq 1.5$ Å^{-1}. The features at higher q are scattering from features within the asphaltene.

Figure 7 shows $S(q)$ of the sulfoxide asphaltene [Figure 1(b)] in each simulated solvent composition. The experimental data in toluene, and an equal mixture of toluene and heptane are also shown, and compared to the closest available simulation results. In pure toluene and 2:8 heptane:toluene, there is low aggregation, and the scattering profiles resemble those from the thiophene systems. As the chemical structures of the asphaltenes are almost identical, any large differences in scattering intensity are a result of changes in aggregation. The experimental data in toluene again match up well with the simulated results in the overlapping q range. In systems with compositions from 4:6 to 10:0, there is a dramatic change in the range $q < 0.5$ Å^{-1}. This is consistent with the snapshots in Figure 4, which show significant clustering in heptane-rich solvents. With 8:2 and 10:0 heptane:toluene solvents, there is a clear portion of power-law behavior in $S(q)$. An object with fractal dimension D has a structure factor $S(q) \sim q^{-D}$.[56] Other experimental studies of asphaltene aggregates using SANS

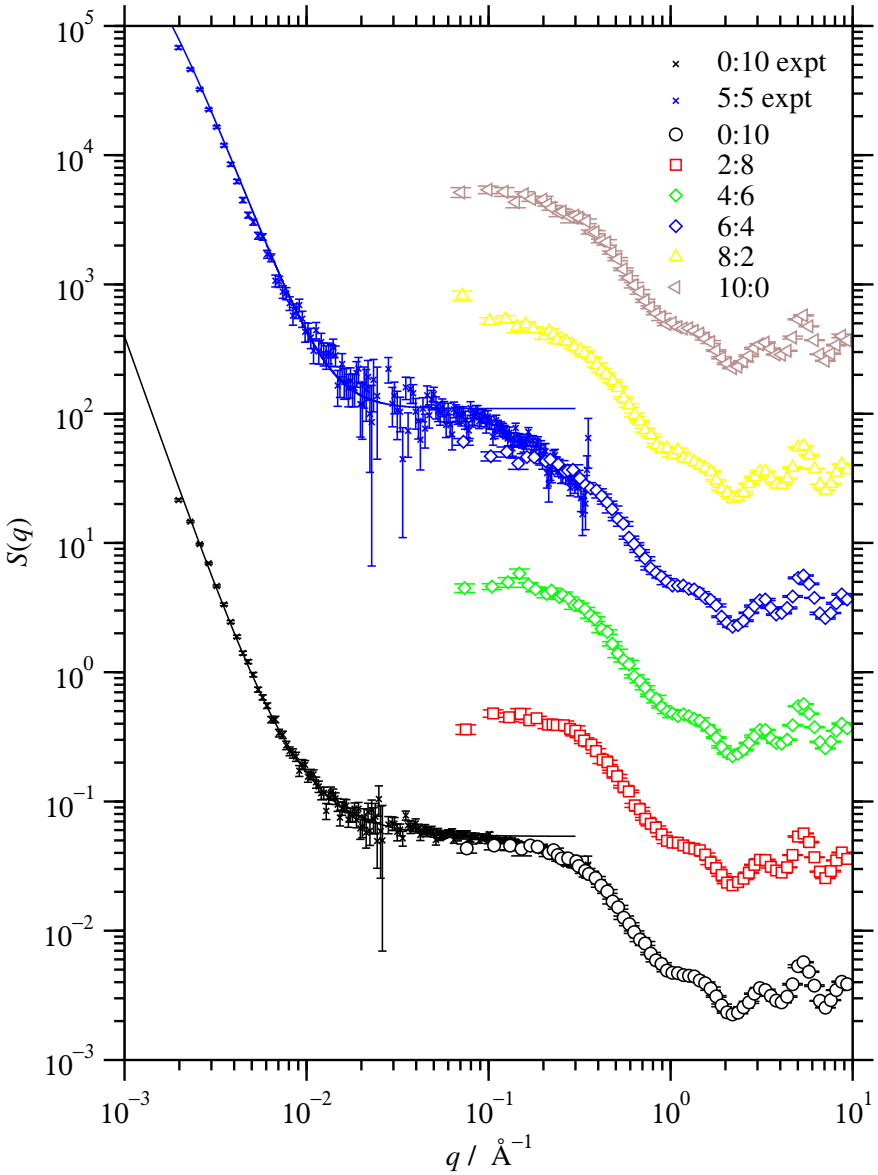

Figure 6: The structure factor, $S(q)$, of the thiophene asphaltene with different solvent compositions. The ratios refer to the heptane:toluene content by volume. The hollow symbols are the simulation results, and the crosses are the experimental measurements scaled to match up with the simulation results. The experimental results were fitted with eq 4. The combined results for each solvent composition are scaled by a successive factor of 10 (and hence shifted by 1 unit on the logarithmic scale) for clarity.

and sedimentation rates give a range of estimates of D, with some around $D = 2$, depending on system composition.[57,58] The simulations are not inconsistent with these results. Fitting an equation of the form $S(q) = A + Bq^{-D}$ in the range $q \geq 0.1$ Å^{-1} gives $D = 2.11(5)$ for the 8:2 system, and $D = 2.23(3)$ for the 10:0 system. The fits are shown in Figure 7. The results from the real 5:5 heptane:toluene mixture show a stronger turnover in the range 0.2 Å$^{-1} < q < 0.5$ Å^{-1}, and $S(q)$ at lower q is below the simulation results, indicating that there are larger clusters in the simulation. This could be due to the higher concentration of asphaltene in the simulated systems as compared to the experiment.

The increase in π–π stacking causes the peak at 1.5 Å^{-1} to becomes more prominent as more heptane is added. In toluene and the 2:8 system there is only a small feature here, due to the low proportion of stacked asphaltenes. As the volume fraction of heptane increases, the peak becomes more prominent. This feature is almost identical in the 6:4, 8:2, and pure-heptane systems, signaling a similar degree of π–π stacking. As with the thiophene, above $q \simeq 1.5$ Å^{-1}, the features in $S(q)$ are almost identical as they come from intramolecular scattering.

Figure 8 shows $S(q)$ for the sulfone asphaltene in toluene, heptane, and intermediate mixtures. As with the other asphaltenes, experimental data are compared to the closest available solvent composition. Looking at the snapshots in Figure 5, in pure toluene, the sulfone asphaltene is more aggregated than the other two asphaltenes. At low q, this is signaled by a larger $S(q)$ than in the thiophene and sulfoxide systems. This also appears in the experimental data, with both profiles showing consistency with the simulation results in the range of overlapping q. The changeover in low q is more gradual than in the sulfoxide system, and occurs between the 4:6 and 6:4 heptane:toluene systems, confirming what is seen visually in the snapshots. The peak at $q \simeq 1.5$ Å^{-1}, corresponding to π–π stacking, is quite prominent in all systems, but increases in height with the proportion of heptane, indicating greater aggregation.

To summarize, structure factors of model asphaltenes in heptane/toluene mixtures from

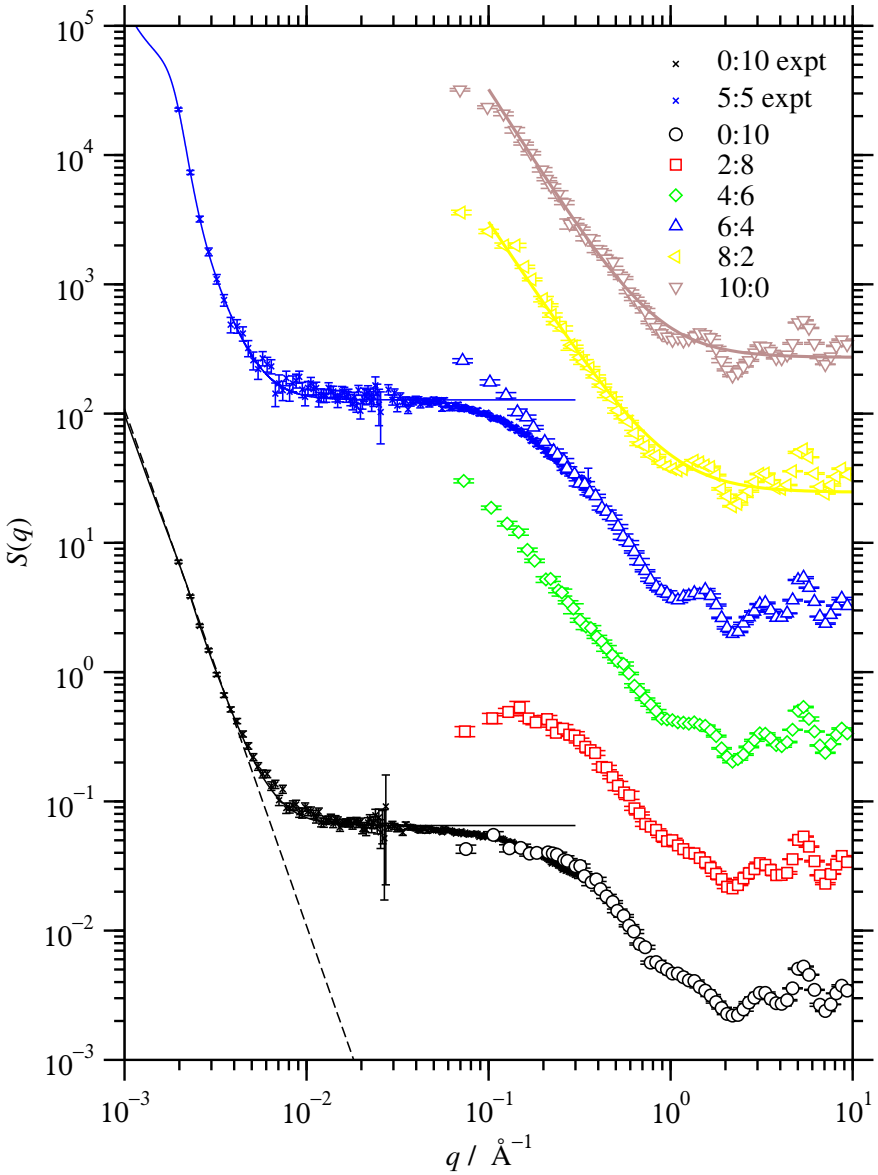

Figure 7: The scattered intensity, $S(q)$, of the sulfoxide asphaltene for different solvent compositions. The ratios refer to the heptane:toluene content by volume. The hollow symbols are the simulation results, and the crosses are the experimental measurements scaled to match up with the simulation results. The experimental results were fitted with eq 4 (solid lines) and the dashed line is proportional to q^{-4}. The simulation results for the 8:2 and 10:0 systems were fitted in the range $q \geq 0.1$ Å^{-1} with a simple power law; see the text for details. The combined results for each solvent composition are scaled by a successive factor of 10 (and hence shifted by 1 unit on the logarithmic scale) for clarity.

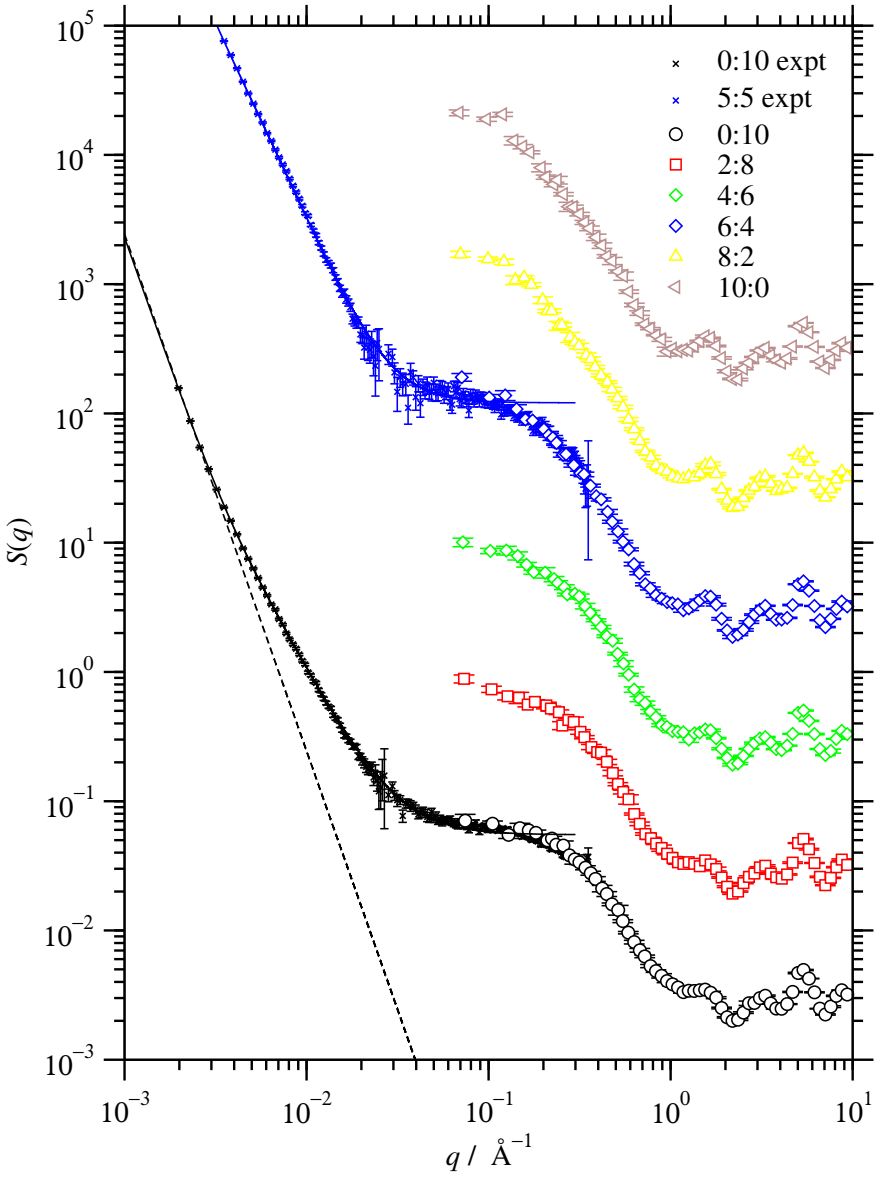

Figure 8: The scattered intensity, $S(q)$, of the sulfone asphaltene in different mixtures of heptane and toluene. The ratios refer to the heptane:toluene content by volume. The hollow symbols are the simulation results, and the crosses are the experimental measurements scaled to match up with the simulation results. The experimental results were fitted with eq 4 (solid lines) and the dashed line is proportional to q^{-4}. The combined results for each solvent composition are scaled by a successive factor of 10 (and hence shifted by 1 unit on the logarithmic scale) for clarity.

MD simulations and SANS experiments have been compared directly and critically. In all cases the simulated scattering profiles are consistent with experimental measurements, giving confidence that the OPLS-AA force-field is able to accurately represent the real clusters. The increase in $S(q)$ at low q with increasing heptane content is consistent with the presence of nanoaggregates, as seen in the simulations, and as described in the Yen-Mullins model.[9,10] Changing the oxidation state of sulfur in the asphaltene has a large effect on the scattering profiles due to the differing levels of aggregation, again as seen directly in the simulations. As far as the authors are aware, such direct comparisons of simulated and experimental scattering from asphaltene aggregates are rare.

3.2.1 Experimental Low-q Behavior

The experimental data at low q ($q < 0.01$ Å^{-1}) can be fitted with a shape independent 'broad-peak' model. In this approach, a Lorentzian-like peak is superimposed on a power-law decay to yield both a characteristic length scale ξ for the nanoaggregates, and an exponent β related to the fractal dimension. The scattering intensity is given by

$$I(q) = \frac{A}{q^{\alpha}} + \frac{B}{1 + (q\xi)^{\beta}} + C, \tag{4}$$

where A is the Porod law scale factor, α is the Porod exponent, B is the Lorentzian scale factor, and C is a q-independent background arising from incoherent scattering and minor instrumental contributions. The first term in eq 4 is constrained to $\alpha = 4$ and corresponds physically to scattering from locally planar interfaces of large particles with sizes $r \gg 1/q$. Adopting this shape-independent model avoids over fitting, particularly in systems with heterogeneous or ill-defined structures, as is the case here. Even using such a shape independent model, there are still large fitting errors in the values of ξ and β, but in most cases ξ is on the order of hundreds of ångströms, and β is between 2 and 3, which are physically reasonably values.

Figure 7 shows that the scattered intensity of sulfoxide aggregates in toluene decays as $I(q) \sim q^{-4}$ below $q \simeq 0.004$ Å^{-1} which indicates the presence of large particles in the system. Figure 8 shows similar behavior for sulfone aggregates in toluene below $q \simeq 0.003$ Å^{-1}. The lack of this power law decay in the thiophene systems indicates an absence of very large particles.

3.3 Radial Distribution Functions

In this section the RDFs of sulfur and oxygen are presented to quantify the internal structure of the aggregates.

Thiophene Figure 9 shows the radial distribution function (eq 1) of the thiophene sulfur atoms in toluene (0:10) and heptane (10:0). In toluene there is a sharp peak at $r \simeq 3.5$ Å, which is approximately the diameter of a sulfur atom. The most common way for these to appear is in pairs of asphaltenes, stacked on top of one another. There is another broad feature around $r \simeq 7.5$ Å, approximately two times the diameter of a sulfur atom, corresponding to the outer sulfur atoms in stacks of three asphaltenes. The peak is broadened as the asphaltenes do not stack perfectly. Above this distance there are no more obvious structural features, and the function decays to the ideal gas limit $g(r) = 1$, indicating that the aggregates tend to be small, with structure limited to the $r < 15$ Å range. The function in heptane is very similar, but with slightly higher peaks, suggesting only slightly more aggregation in heptane, and this is in agreement with the simulation snapshots, cluster distributions, and $S(q)$.

Sulfoxide Figure 10 shows the sulfur-sulfur and sulfur-oxygen RDFs in pure toluene and in pure heptane. In toluene, the first peak in $g_{\mathrm{SS}}(r)$ appears at $r \simeq 4.5$ Å, which is larger than in the thiophene system. This distance corresponds to two sulfur atoms separated by an oxygen atom. The height of the peak is about $g_{\mathrm{SS}}(4.5 \text{ Å}) = 15$, roughly equal to that in the thiophene system, implying a similar level of aggregation. This agrees with the snapshots and $S(q)$. In heptane, the form of $g_{\mathrm{SS}}(r)$ is the same but with taller peaks. The first peak has

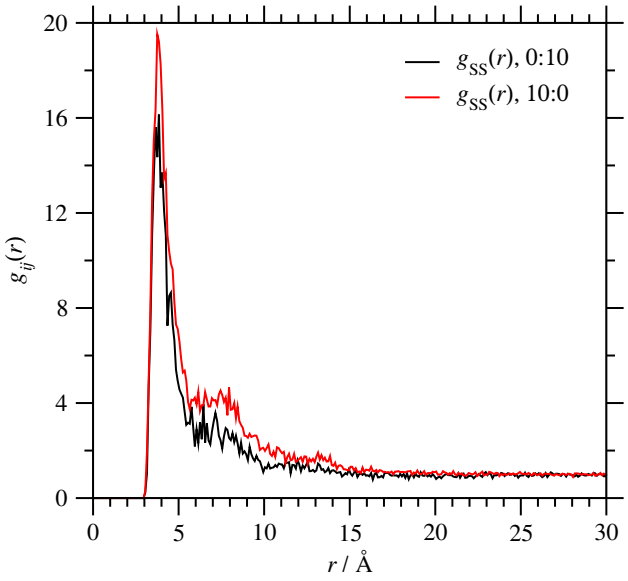

Figure 9: The RDF of the sulfur atoms in the thiophene asphaltene in toluene (0:10) and heptane (10:0).

a height of roughly 135 and a shoulder at 3.5 Å, which is a result of the sulfoxide groups being oriented in opposite directions, with the oxygen atoms pointing away from one another. The shoulder is small as the corresponding configuration brings the partially positively charged sulfur atoms closer together, and the electrostatic repulsion makes this less favorable than having alternating sulfur and oxygen atoms.

The oxygen-sulfur RDF, $g_{\mathrm{SO}}(r)$ has the same form in toluene and heptane, but all features are less pronounced in toluene, as there is less aggregation. The case in heptane will be discussed in more detail, since the features in $g_{\mathrm{SO}}(r)$ are much clearer. Figure 11(a) shows a schematic diagram of the distances corresponding to features in $g_{\mathrm{SO}}(r)$. The sharp peak at $r \simeq 1.5$ Å is a result of the bonded sulfur-oxygen pairs. The peaks at 3 Å and 6 Å come from the inner and outer pair of sulfur and oxygen atoms that result when the functional groups arrange themselves in the 'head-to-tail' configuration; an example cluster, highlighting the polar organization of the S=O groups, can be seen in Figure 11(b). Similarly the features at 7.5 Å and 10.5 Å are from the inner and outer sulfur-oxygen pairs in a chain of three sulfoxide groups. The peaks get broader at larger r due to contributions from other arrangements of asphaltenes, as well as fluctuations and flexibility within the aggregate. The differences

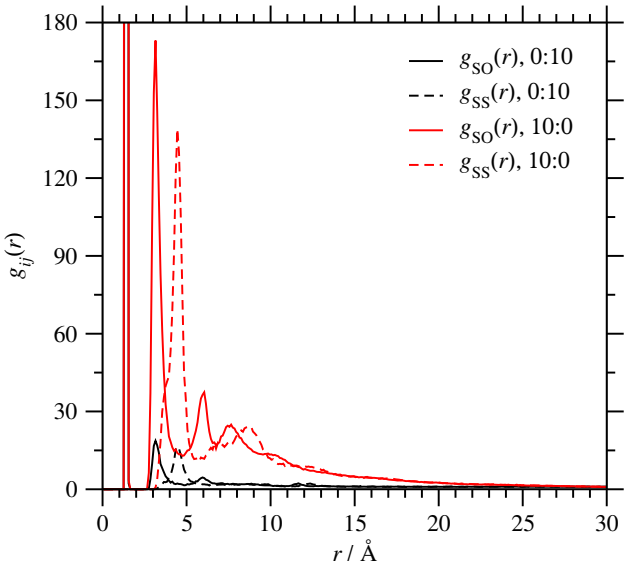

Figure 10: The partial RDFs for sulfur-sulfur pairs $g_{SS}(r)$ (dashed lines), and sulfur-oxygen pairs $g_{SO}(r)$ (solid lines) of the sulfoxide asphaltene, in toluene (0:10) and heptane (10:0).

between the toluene and heptane functions are mainly in the intensity of the peaks. In toluene the first two peaks are clearly visible, but the function decays very quickly, showing very little long range correlation between the functional groups. In heptane, $g_{SO}(r)$ shows structure up to the feature at $r = 10.5$ Å, and does not decay to 1 until $r \simeq 25$ Å. This is consistent with the apparent diameter of a nanoaggregate as shown in the simulation snapshots.

Sulfone Figure 12 shows the RDFs for the sulfur-sulfur and sulfur-oxygen pairs in heptane and toluene. In heptane, $g_{SS}(r)$ has its first peak at $r = 5$ Å, which is slightly larger distance than in sulfoxide. It does not have a shoulder at $r \simeq 3.5$ Å because the sulfone functional group has C_{2v}-like symmetry, i.e., the flipped geometry is almost equivalent. The next peak, at $r \simeq 8$ Å, is at a shorter distance than in the sulfoxide because the sulfur and oxygen no longer only form chains of alternating sulfur and oxygen atoms. As the sulfur is bonded to two oxygen atoms, it is possible to form branched structures. This could be one reason for the higher prevalence of sulfone nanoaggregates, as compared to sulfoxide, in systems with a low heptane content, by providing more points of contact for the asphaltenes to aggregate. The final peak at $r \simeq 11$ Å is from the 'head-to-tail' stacking configuration.

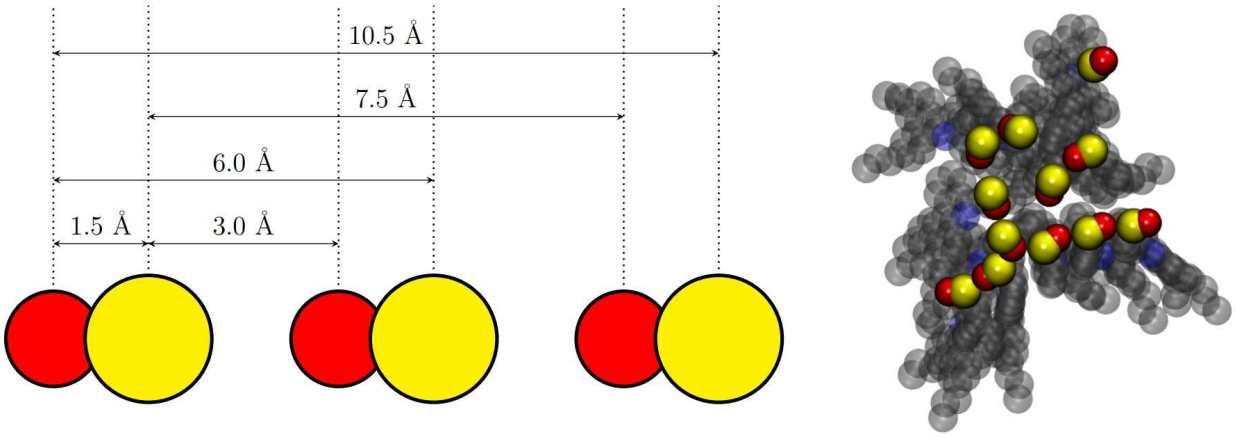

(a) (b)

Figure 11: (a) A schematic diagram of a chain of S=O groups, indicating the positions of the peaks in the corresponding RDF. The red and yellow circles represent oxygen, and sulfur atoms, respectively. The distances between atoms fluctuate during the simulation, but the average values (corresponding to the peaks in the RDF) are given. (b) A snapshot of sulfoxide-asphaltene aggregates in pure heptane, highlighting the polar organization of the S=O groups.

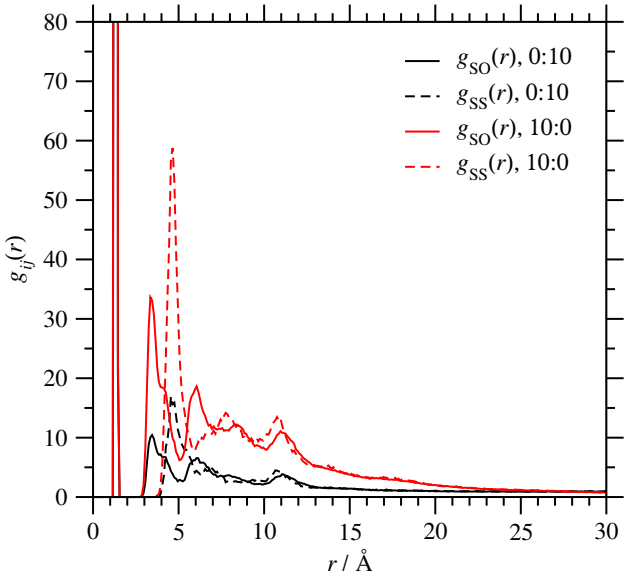

Figure 12: The partial RDFs for sulfur-sulfur pairs $g_{SS}(r)$ (dashed lines), and sulfur-oxygen pairs $g_{SO}(r)$ (solid lines) of the sulfone asphaltene, in toluene (0:10) and heptane (10:0).

$g_{SO}(r)$ shows similar features to those for the sulfoxide. Note that in the sulfone system, since there are two oxygen atoms bonded to the sulfur, the normalization factor in eq 1 is doubled, resulting in reduced peak heights. As with sulfoxide, the peak at $r \simeq 1.5$ Å comes from bonded pairs. The second peak at $r \simeq 3.5$ Å is from the first non-bonded sulfur-oxygen pair. The shoulder in the peak is from the other oxygen associated with the same functional group. There are contributions to $g_{SO}(r)$ from the same structural motifs as in Figure 11(a), however these peaks are broadened by the presence of the extra oxygen atoms, and by the branched aggregation modes mentioned above. In particular, the peak at $r \simeq 11$ Å is much more prominent in the sulfone system due to the branching. $g_{SS}(r)$ approaches 1 at $r \simeq 25$ Å in heptane, and at $r \simeq 15$ Å in toluene, consistent with the nanoaggregate sizes shown in Figures 5(a) and (f).

4 Conclusions

The structures and aggregation of three different model asphaltenes in heptane-toluene mixtures have been studied using molecular-dynamics simulations and small-angle neutron scattering experiments. Each asphaltene contains a sulfur-containing functional group. Changing the oxidation state of that sulfur atom is found to have dramatic effects on both the structure of the aggregates and the level of heptane required to trigger the formation of large clusters. The benzothiophene asphaltene forms nanoaggregates in both toluene and heptane, which have similar structures in both solvents. The sulfoxide functionalized asphaltene forms nanoaggregates in toluene, but large clusters in solvents above 40% by volume of heptane. The tendency of the polar sulfoxide group to associate with other sulfoxide groups is a key factor in the stability of the aggregates, showing the important role of electrostatic forces in aggregation in non-aqueous media. Sulfone functionalized asphaltenes form larger nanoaggregates in toluene than sulfoxide, and correspondingly larger clusters above 40% by volume of heptane. The aggregates are also strongly stabilized by the electrostatic inter-

actions between the sulfone functionality. This fits in with the current understanding that asphaltene precipitation is not caused by π–π stacking alone, and that other functionality in the molecule plays a very important role. This is important knowledge when developing dispersants to stabilize asphaltene nanoaggregates in solution.

Experimental neutron-scattering profiles compare favorably to those calculated from simulation, although direct comparisons are limited to a narrow range of q due to the different length scales being probed. There is a changeover in low q corresponding to the onset of aggregation in the model asphaltenes. Scaling behavior is observed in the sulfoxide simulations, and is consistent with previous experimental determinations of the apparent mass fractal dimension of asphaltene clusters. Insofar as direct comparisons are feasible, the consistency between simulated and experimental data gives confidence that the OPLS-AA force field can be used to model real-life asphaltene systems accurately.

Finally, the radial distribution functions of the sulfur and oxygen atoms were calculated in order to characterize the internal structure and binding modes of the asphaltene clusters. In the thiophene functionalized molecule there was a small tendency of the sulfur atoms to associate, but the structure was very similar in both heptane and toluene. Chains of alternating sulfur and oxygen atoms were identified in clusters of the sulfoxide asphaltene. This energetically favorable conformation contributes strongly to the stability of the clusters. The two oxygen atoms in the sulfone asphaltene were found to be structurally important. Chains of alternating oxygen and sulfur atoms are formed, as in the sulfoxide clusters, but the extra oxygen also allows 'branching' of these chains.

Acknowledgement

This research was funded jointly by Infineum UK Ltd and the Engineering and Physical Sciences Research Council (EPSRC). J. G. C. was supported by an EPSRC DTP CASE studentship (Project Reference EP/T517884/1). C. H. was supported by the EPSRC Centre

for Doctoral Training in Molecules to Product (Project Reference EP/S022473/1).

Data Availability

A sample LAMMPS input file, sample LAMMPS data files for each asphaltene in 2:8 heptane:toluene mixtures, and the raw data plotted in Figures 3, 6, 7, 8, 9, 10, and 12 [will be] openly available from the School of Chemistry Collection in Edinburgh DataShare at `https://datashare.ed.ac.uk/handle/10283/746`.

References

(1) Alshareef, A. H. Asphaltenes: Definition, Properties, and Reactions of Model Compounds. *Energy Fuels* **2020**, *34*, 16–30.

(2) Liu, Y.; Cao, W. Rejuvenating Oxidized Paving Asphalts – When Softeners Meet Asphaltene Dispersants. *Fuel* **2024**, *363*, 130948.

(3) Yuan, B.; Wood, D. A. *Formation Damage During Improved Oil Recovery: Fundamentals and Applications*, 1st ed.; Gulf Professional Publishing, 2018.

(4) Alimohammadi, S.; Zendehboudi, S.; James, L. A Comprehensive Review of Asphaltene Deposition in Petroleum Reservoirs: Theory, Challenges, and Tips. *Fuel* **2019**, *252*, 753–791.

(5) Bartle, K. D.; Jones, J. M.; Lea-Langton, A. R.; Pourkashanian, M.; Ross, A. B.; Thillaimuthu, J. S.; Waller, P. R.; Williams, A. The Combustion of Droplets of High-Asphaltene Heavy Oils. *Fuel* **2013**, *103*, 835–842.

(6) Sultanbekov, R.; Islamov, S.; Mardashov, D.; Beloglazov, I.; Hemmingsen, T. Research of the Influence of Marine Residual Fuel Composition on Sedimentation Due to Incompatibility. *J. Mar. Sci. Eng.* **2021**, *9*, 1067.

(7) Mullins, O. C. The Asphaltenes. *Annu. Rev. Anal. Chem* **2011**, *4*, 393–418.

(8) Bake, K. D.; Craddock, P. R.; Bolin, T. B.; Abdallah, W.; Mitra-Kirtley, S.; Andrews, A. B.; Mullins, O. C.; Pomerantz, A. E. Structure-Solubility Relationships in Coal, Petroleum, and Immature Source-Rock-Derived Asphaltenes. *Energy & Fuels* **2020**, *34*, 10825–10836.

(9) Dickie, J. P.; Yen, T. F. Macrostructures of the Asphaltic Fractions by Various Instrumental Methods. *Anal. Chem.* **1967**, *39*, 1847–1852.

(10) Mullins, O. C. The Modified Yen Model. *Energy Fuels* **2010**, *24*, 2179–2207.

(11) Mullins, O. C. et al. Advances in Asphaltene Science and the Yen–Mullins Model. *Energy Fuels* **2012**, *26*, 3986–4003.

(12) Murgich, J. Intermolecular Forces in Aggregates of Asphaltenes and Resins. *Petrol. Sci. Technol.* **2002**, *20*, 983–997.

(13) Andersen, S. I.; Jensen, J. O.; Speight, J. G. X-ray Diffraction of Subfractions of Petroleum Asphaltenes. *Energy Fuels* **2005**, *19*, 2371–2377.

(14) Gray, M. R.; Tykwinski, R. R.; Stryker, J. M.; Tan, X. Supramolecular Assembly Model for Aggregation of Petroleum Asphaltenes. *Energy Fuels* **2011**, *25*, 3125–3134.

(15) Zhang, Y.; Siskin, M.; Gray, M. R.; Walters, C. C.; Rodgers, R. P. Mechanisms of Asphaltene Aggregation: Puzzles and a New Hypothesis. *Energy Fuels* **2020**, *34*, 9094–9107.

(16) Speight, J. Petroleum Asphaltenes – Part 1: Asphaltenes, Resins and the Structure of Petroleum. *Oil Gas Sci. Technol.* **2004**, *59*, 467–477.

(17) George, G. N.; Gorbaty, M. L. Sulfur K-edge X-ray Absorption Spectroscopy of Petroleum Asphaltenes and Model Compounds. *J. Am. Chem. Soc.* **1989**, *111*, 3182–3186.

(18) Kasrai, M.; Bancroft, G. M.; Brunner, R.; Connan, J. The Chemical Nature of Oxidized Sulphur in Asphaltenes from X-Ray Absorption Spectroscopy. *J. Phys. IV France* **1997**, *7*, C2–809–C2–810.

(19) Mitra-Kirtley, S.; Mullins, O. C.; Ralston, C. Y.; Sellis, D.; Pareis, C. Determination of Sulfur Species in Asphaltene, Resin, and Oil Fractions of Crude Oils. *Appl. Spectrosc.* **1998**, *52*, 1522–1525.

(20) Pomerantz, A. E.; Seifert, D. J.; Bake, K. D.; Craddock, P. R.; Mullins, O. C.; Kodalen, B. G.; Mitra-Kirtley, S.; Bolin, T. B. Sulfur Chemistry of Asphaltenes from a Highly Compositionally Graded Oil Column. *Energy Fuels* **2013**, *27*, 4604–4608.

(21) Bava, Y. B.; Geronés, M.; Giovanetti, L. J.; Andrini, L.; Erben, M. F. Speciation of Sulphur in Asphaltenes and Resins from Argentinian Petroleum by Using XANES Spectroscopy. *Fuel* **2019**, *256*, 115952.

(22) Li, M.; Chen, X.; Chen, W.; Wang, J.; Zhang, L. The Effect of Low-Temperature Oxidation on Asphaltene Structure and Properties During Air Injection. *Fuel* **2023**, *352*, 129051.

(23) Greenfield, M. L.; Byrne, M.; Mitra-Kirtley, S.; Kercher, E. M.; Bolin, T. B.; Wu, T.; Craddock, P. R.; Bake, K. D.; Pomerantz, A. E. XANES Measurements of Sulfur Chemistry During Asphalt Oxidation. *Fuel* **2015**, *162*, 179–185.

(24) Hutchinson, C. J.; Dowding, P. J.; Heyam, A.; Pask, C. M.; Robinson, T. P.; Harbottle, D.; Marsden, S. P. Synthesis and Characterisation of Dibenzo[a,c]phenanthridines as Model Asphaltenes. (in preparation).

(25) Barré, L.; Jestin, J.; Morisset, A.; Palermo, T.; Simon, S. Relation Between Nanoscale Structure of Asphaltene Aggregates and Their Macroscopic Solution Properties. *Oil Gas Sci. Technol.* **2009**, *64*, 617–628.

(26) Eyssautier, J.; Levitz, P.; Espinat, D.; Jestin, J.; Gummel, J.; Grillo, I.; Barré, L. Insight Into Asphaltene Nanoaggregate Structure Inferred by Small Angle Neutron and X-ray Scattering. *J. Phys. Chem. B* **2011**, *115*, 6827–6837.

(27) Sodero, A. C. R.; Santos Silva, H.; Guevara Level, P.; Bouyssiere, B.; Korb, J.-P.; Carrier, H.; Alfarra, A.; Bégué, D.; Baraille, I. Investigation of the Effect of Sulfur Heteroatom on Asphaltene Aggregation. *Energy Fuels* **2016**, *30*, 4758–4766.

(28) Santos Silva, H.; Sodero, A. C. R.; Bouyssiere, B.; Carrier, H.; Korb, J.-P.; Alfarra, A.; Vallverdu, G.; Bégué, D.; Baraille, I. Molecular Dynamics Study of Nanoaggregation in Asphaltene Mixtures: Effects of the N, O, and S Heteroatoms. *Energy Fuels* **2016**, *30*, 5656–5664.

(29) Santos Silva, H.; Alfarra, A.; Vallverdu, G.; Bégué, D.; Bouyssiere, B.; Baraille, I. Sensitivity of Asphaltene Aggregation toward the Molecular Architecture under Desalting Thermodynamic Conditions. *Energy Fuels* **2018**, *32*, 2681–2692.

(30) Santos Silva, H.; Alfarra, A.; Vallverdu, G.; Bégué, D.; Bouyssiere, B.; Baraille, I. Asphaltene Aggregation Studied by Molecular Dynamics Simulations: Role of the Molecular Architecture and Solvents on the Supramolecular or Colloidal Behavior. *Pet. Sci.* **2019**, *16*, 669–684.

(31) Santos Silva, H.; Alfarra, A.; Vallverdu, G.; Bégué, D.; Bouyssiere, B.; Baraille, I. Impact of H-Bonds and Porphyrins on Asphaltene Aggregation As Revealed by Molecular Dynamics Simulations. *Energy Fuels* **2018**, *32*, 11153–11164.

(32) Headen, T. F.; Boek, E. S.; Jackson, G.; Totton, T. S.; Müller, E. A. Simulation of Asphaltene Aggregation through Molecular Dynamics: Insights and Limitations. *Energy Fuels* **2017**, *31*, 1108–1125.

(33) Javanbakht, G.; Sedghi, M.; Welch, W. R.; Goual, L.; Hoepfner, M. P. Molecular

Polydispersity Improves Prediction of Asphaltene Aggregation. *J. Mol. Liq.* **2018**, *256*, 382–394.

(34) Pétuya, R.; Punase, A.; Bosoni, E.; de Oliveira Filho, A. P.; Sarria, J.; Purkayastha, N.; Wylde, J. J.; Mohr, S. Molecular Dynamics Simulations of Asphaltene Aggregation: Machine-Learning Identification of Representative Molecules, Molecular Polydispersity, and Inhibitor Performance. *ACS Omega* **2023**, *8*, 4862–4877.

(35) Hashmi, S. M.; Quintiliano, L. A.; Firoozabadi, A. Polymeric Dispersants Delay Sedimentation in Colloidal Asphaltene Suspensions. *Langmuir* **2010**, *26*, 8021–8029.

(36) Firoozinia, H.; Abad, K. F. H.; Varamesh, A. A Comprehensive Experimental Evaluation of Asphaltene Dispersants for Injection Under Reservoir Conditions. *Pet. Sci.* **2016**, *13*, 280–291.

(37) Mojica, D.; Angeles, M.; Alvarez, O.; Pradilla, D. Asphaltene Precipitation and the Influence of Dispersants and Inhibitors on Morphology Probed by AFM. *Colloids Interfaces* **2023**, *7*, 3.

(38) Zhao, Z.; Xia, X.; Li, Y.; Liu, D.; Cai, W.; Li, C.; Sun, G.; Yao, B.; Yang, F. Effect of Dodecylbenzenesulfonic Acid as an Asphaltene Dispersant on the W/O Emulsion Stabilized by Asphaltenes and Paraffin Wax. *Energy Fuels* **2023**, *37*, 4244–4255.

(39) Lowry, E.; Sedghi, M.; Goual, L. Polymers for Asphaltene Dispersion: Interaction Mechanisms and Molecular Design Considerations. *J. Mol. Liq.* **2017**, *230*, 589–599.

(40) Jorgensen, W. L.; Madura, J. D.; Swenson, C. J. Optimized Intermolecular Potential Functions for Liquid Hydrocarbons. *J. Am. Chem. Soc.* **1984**, *106*, 6638–6646.

(41) Jorgensen, W. L.; Maxwell, D. S.; Tirado-Rives, J. Development and Testing of the OPLS All-Atom Force Field on Conformational Energetics and Properties of Organic Liquids. *J. Am. Chem. Soc.* **1996**, *118*, 11225–11236.

(42) Rackers, J. A.; Wang, Z.; Lu, C.; Laury, M. L.; Lagardère, L.; Schnieders, M. J.; Piquemal, J.-P.; Ren, P.; Ponder, J. W. Tinker 8: Software Tools for Molecular Design. *J. Chem. Theory Comput.* **2018**, *14*, 5273–5289.

(43) Tinker – Software Tools for Molecular Design. `https://dasher.wustl.edu/tinker/`, 2025.

(44) Jorgensen, W. L.; Tirado-Rives, J. Potential Energy Functions for Atomic-Level Simulations of Water and Organic and Biomolecular Systems. *Proc. Nat. Acad. Sci. USA* **2005**, *102*, 6665–6670.

(45) Dodda, L. S.; Vilseck, J. Z.; Tirado-Rives, J.; Jorgensen, W. L. 1.14*CM1A-LBCC: Localized Bond-Charge Corrected CM1A Charges for Condensed-Phase Simulations. *J. Phys. Chem. B* **2017**, *121*, 3864–3870.

(46) Dodda, L. S.; Cabeza de Vaca, I.; Tirado-Rives, J.; Jorgensen, W. L. LigParGen Web Server: An Automatic OPLS-AA Parameter Generator for Organic Ligands. *Nucleic Acids Res.* **2017**, *45*, W331–W336.

(47) LigParGen. `https://traken.chem.yale.edu/ligpargen/`, 2025.

(48) Martínez, L.; Andrade, R.; Birgin, E. G.; Martínez, J. M. PACKMOL: A Package for Building Initial Configurations for Molecular Dynamics Simulations. *J. Comput. Chem.* **2009**, *30*, 2157–2164.

(49) Thompson, A. P.; Aktulga, H. M.; Berger, R.; Bolintineanu, D. S.; Brown, W. M.; Crozier, P. S.; in't Veld, P. J.; Kohlmeyer, A.; Moore, S. G.; Nguyen, T. D.; Shan, R.; Stevens, M. J.; Tranchida, J.; Trott, C.; Plimpton, S. J. LAMMPS – a Flexible Simulation Tool for Particle-Based Materials Modeling at the Atomic, Meso, and Continuum Scales. *Comput. Phys. Commun.* **2022**, *271*, 108171.

(50) LAMMPS Molecular Dynamics Simulator. http://www.lammps.org, 2025.

(51) Brown, M. W.; Wang, P.; Plimpton, S. J.; Tharrington, A. N. Implementing Molecular Dynamics on Hybrid High Performance Computers – Short Range Forces. *Comput. Phys. Commun.* **2011**, *182*, 898–911.

(52) Lemmon, E. W.; Bell, I. H.; Huber, M. L.; McLinden, M. O. In *NIST Chemistry WebBook, NIST Standard Reference Database Number 69*; Linstrom, P. J., Mallard, W. G., Eds.; National Institute of Standards and Technology, Gaithersburg MD, 20899, 2024.

(53) Ghanavati, M.; Shojaei, M.; Ramazani, S. A. A. Effects of Asphaltene Content and Temperature on Viscosity of Iranian Heavy Crude Oil: Experimental and Modeling Study. *Energy Fuels* **2013**, *27*, 7217–7232.

(54) Squires, G. L. *Introduction to the Theory of Thermal Neutron Scattering*; Dover Publications Inc., 1997.

(55) Rumble, J. R., Ed. *CRC Handbook of Chemistry and Physics*, 106th ed.; CRC Press: Boca Raton, 2024.

(56) Chaikin, P. M.; Lubensky, T. C. *Principles of Condensed Matter Physics*; Cambridge University Press: Cambridge, 1995.

(57) Hoepfner, M. P.; Fávero, C. V. B.; Haji-Akbari, N.; Fogler, H. S. The Fractal Aggregation of Asphaltenes. *Langmuir* **2013**, *29*, 8799–8808.

(58) Rahmani, N. H. G.; Dabros, T.; Masliyah, J. H. Settling Properties of Asphaltene Aggregates. *Energy Fuels* **2005**, *19*, 1099–1108.

TOC Graphic

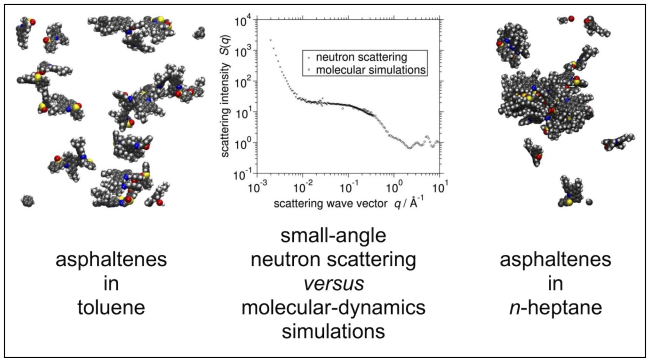
neutron scattering
molecular simulations
scattering intensity S(q)
scattering wave vector q / Å-1
asphaltenes in toluene
small-angle neutron scattering versus molecular-dynamics simulations
asphaltenes in n-heptane